

# Parametric Lattice Boltzmann Method

Jae Wan Shim\*

*KIST and University of Science and Technology*

(Dated: February 25, 2014)

## Abstract

The discretized equilibrium distributions of the lattice Boltzmann method are presented by using the coefficients of the Lagrange interpolating polynomials that pass through the points related to discrete velocities and using moments of the Maxwell-Boltzmann distribution. The ranges of flow velocity and temperature providing positive valued distributions vary with regulating discrete velocities as parameters. In addition, thermal flows are simulated by only five on-lattice discrete velocities and the distributions upon asymmetric sets of discrete velocities are introduced.

---

\* jae-wan.shim@m4x.org

One way of simulating fluid flows is to use artificial particles jumping from one node to another in a regular lattice with a limited number of discrete velocities as in the lattice Boltzmann method [1–6]. At a given node  $x$  and time  $t$ , the existence of a particle having a given discrete velocity  $v_i$  is expressed by a velocity distribution probability  $p_i(x, t)$  in real numbers instead of zero or one. Particles collide with each other every time step  $\Delta t$  and thus velocity distributions change according to a redistribution rule  $r_i(x, t)$  within the following discretized advection formula having a single relaxation constant  $\omega$  as

$$f_i(x + v_i \Delta t, t + \Delta t) = (1 - \omega) f_i(x, t) + \omega F_i(x, t) \quad (1)$$

where  $f_i(x, t)$  is the density of the particles having  $v_i$ , hence it is expressed by total density  $\rho(x, t)$  as  $\rho(x, t) p_i(x, t)$ , and  $F_i(x, t) = \rho(x, t) r_i(x, t)$  which is called the discretized equilibrium distribution. The constitution of  $F_i(x, t)$  with corresponding discrete velocities  $v_i$  affects the accuracy, efficiency, and stability of the lattice Boltzmann method.

Here, we present parametric discretized equilibrium distributions  $F_i$  or redistribution rules  $r_i = F_i/\rho$  as

$$r_i = \sum_{j=1}^q c_{ij} \mu_{j-1} \quad (2)$$

where  $c_{ij}$  is the coefficient corresponding to the term of degree  $j - 1$  of the Lagrange interpolating polynomial that passes through  $(v_k, \delta_{ik})$  for  $k = 1, 2, \dots, q$  in which  $\delta_{ik}$  is the Kronecker delta and  $\mu_n$  is the  $n$ th moment of the Maxwell-Boltzmann distribution  $F(v)$  defined by  $\mu_n = \int v^n F(v) dv$ . By defining  $\hat{\mu}_n = \sum v_i^n r_i$ , this rule satisfies the  $n$ th moment identity  $\hat{\mu}_n = \mu_n$  for  $n = 0, 1, \dots, q - 1$  in one-dimensional space. The detailed derivation is provided in Appendix. Multi-dimensional models can be obtained by tensor products of one-dimensional models or be directly derived from Eq. (A.1) with proper choices of discrete velocities and a desired accuracy.

As an example, the redistribution rule of a model consisting of three discrete velocities  $v_1 = 0$  and  $v_{2,3} = \pm \sqrt{\zeta \theta_0}$  with a reference temperature  $\theta_0$  can be expressed by

$$r_i = w_i \left[ 1 + \frac{v_i u}{\theta_0} + \frac{u^2}{(\zeta - 1) \theta_0^2} (v_i^2 - \theta_0) \right] \quad (3)$$

with  $w_1 = 1 - 1/\zeta$  and  $w_{2,3} = 1/(2\zeta)$  where  $u$  is flow velocity distinguished from particle velocity  $v$  and its discretized one  $v_i$ . Note two values of the parameter  $\zeta = 3$  and  $4$ . With the former, we recover the classical equilibrium distribution called the lattice Bhatnagar-Gross-Krook (LBGK) model [6], and with the latter, we find a more stable model in which

the range of  $u$  providing  $r_i \geq 0$  is wider than any other value of  $\zeta$ . We will demonstrate its enhanced stability by a simulation of the Riemann problem of the shock tube and will discuss its accuracy.

As another example, thermal compressible flows of the Navier-Stokes equations can be simulated by only five on-lattice discrete velocities in one-dimensional space with the following rule and by 25 in two-dimensional space via tensor products. For a symmetric set of discrete velocities defined by  $v_1 = 0$ ,  $v_{2,3} = \pm x$ , and  $v_{4,5} = \pm y$ , the corresponding explicit expression of  $r_i$  is

$$r_1 = \frac{\mu_0 x^2 y^2 - \mu_2 (x^2 + y^2) + \mu_4}{x^2 y^2}, \quad (4a)$$

$$r_{2,3} = \frac{-\mu_1 v_i y^2 - \mu_2 y^2 + \mu_3 v_i + \mu_4}{2v_i^2 (v_i^2 - y^2)}, \quad (4b)$$

$$r_{4,5} = \frac{-\mu_1 v_i x^2 - \mu_2 x^2 + \mu_3 v_i + \mu_4}{2v_i^2 (v_i^2 - x^2)}. \quad (4c)$$

According to the Gauss-Hermite quadrature in the lattice Boltzmann theory [7, 8], we can simulate thermal flows with five discrete velocities obtained from the zeros  $z_i$  of the Hermite polynomial of degree five [9], however, there is an important difference. While the ratios between  $z_i (\neq 0)$  are not always rational so that artificial particles are not allowed to jump from one node to another in a regular lattice, the discrete velocities obeying the rule of Eq. (2) are allowed to do so – we call them on-lattice velocities – by regulating  $x$  and  $y$  such as  $y = 2x$  in Eq. (4). For the on-lattice models, the conventional minimal sets consist of seven velocities for one-dimensional space [10], and 37 velocities [11] or sparse 33 velocities [12, 13] for two-dimensional space in contrast to 25 velocities presented in this paper.

Let us define dimensionless variables  $\bar{u} = u/\sqrt{\theta_0}$ ,  $\bar{v}_i = v_i/\sqrt{\theta_0}$ , and  $\bar{\theta} = \theta/\theta_0$  for simplicity and examine Eq. (3). The contour plot of  $r_i$  with respect to  $\bar{u}$  and  $\bar{v}_2$  is shown in Fig. 1. The shadow area represents the domains providing  $r_i \geq 0$ . The lower boundary curve passing through the points  $P_2$  and  $P_3$  satisfies  $r_1 = 0$ , and the two upper boundaries satisfies  $r_{2,3} = 0$ . We observe that the range of  $\bar{u}$  satisfying  $r_i \geq 0$  for all  $i$  is maximized when  $\zeta = 4$  or  $\bar{v}_2 = 2$  by which  $P_1$  is touched and the range becomes  $|\bar{u}| \leq \sqrt{3}$ . Note that the range of the LBGK model is  $|\bar{u}| \leq \sqrt{2}$  and it is achieved when  $\zeta = 3$ .

We demonstrate the enhanced stability of the parametric lattice Boltzmann model with  $\zeta = 4$  with a simulation of the Riemann problem of the shock tube. We use one thousand nodes for the linear shock tube. The initial condition is set by  $C_L = \{\bar{\rho}_L, \bar{u}_L, \bar{\theta}_L\} = \{6, 0, 1\}$

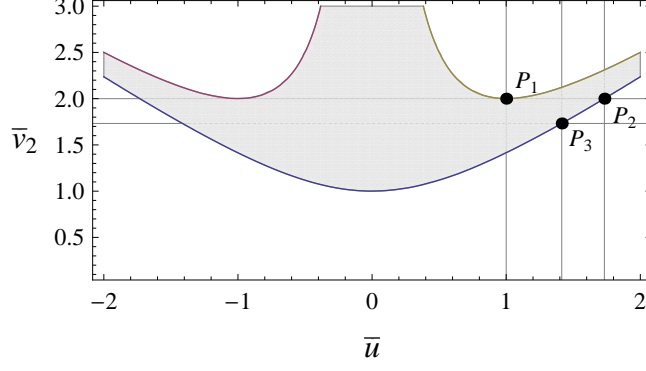


FIG. 1. (Color online) The redistribution rule  $r_i$  of three discrete velocities is drawn. The shadow area represents  $r_i \geq 0$ . The lower boundary passing through the points  $P_2$  and  $P_3$  represents  $r_1 = 0$  and the two upper boundaries represent  $r_{2,3} = 0$ . The point  $P_1 = (1, 2)$  is touched by  $\bar{v}_2 = 2$  or  $\zeta = 4$ . The points  $P_2 = (\sqrt{3}, 2)$  and  $P_3 = (\sqrt{2}, \sqrt{3})$  are the cross points of  $\bar{v}_2 = 2$  (parametric model with  $\zeta = 4$ ) and  $\bar{v}_2 = \sqrt{3}$  (LBGK model) with respect to  $r_1 = 0$ , respectively.

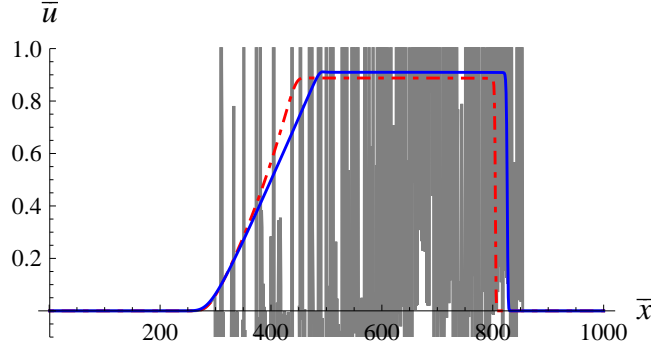


FIG. 2. (Color online) The velocity profiles obtained by the LBGK model (gray oscillating), the parametric model with  $\zeta = 4$  (solid blue), and the entropic model (red dot-dashed) are drawn. The initial density of the left half space is  $\bar{\rho}_L = 6$  and that of the right is  $\bar{\rho}_R = 1$ . For the whole space, the initial velocity and temperature are  $\bar{\theta}_{L,R} = 1$  and  $\bar{u}_{L,R} = 0$ .

for the left half space and  $C_R = \{\bar{\rho}_R, \bar{u}_R, \bar{\theta}_R\} = \{1, 0, 1\}$  for the right where  $\bar{\rho}$  is relative density with respect to a reference. Relative pressure  $\bar{p}$  is obtained by the equation of state of ideal gas  $\bar{p} = \bar{\rho}\bar{\theta}$ . The physical properties of the extreme left and right are maintained by  $C_L$  and  $C_R$ , respectively. Fig. 2 shows the results obtained by three different models; the parametric lattice Boltzmann model with  $\zeta = 4$ , the LBGK model [6] that is equivalent to the parametric model with  $\zeta = 3$ , and the model obtained by an entropy function [14].

TABLE I. The second and the third moments of the Maxwell-Boltzmann distribution, the LBGK, the parametric with  $\zeta = 4$ , and the entropic models are listed.

Model	2nd-order	3rd-order
Maxwell-Boltzmann <sup>a</sup>	$\theta_0 + u^2$	$3\theta_0 u + u^3$
LBGK( $\zeta = 3$ )	$\theta_0 + u^2$	$3\theta_0 u$
Parametric( $\zeta = 4$ )	$\theta_0 + u^2$	$4\theta_0 u$
Entropic	$-\theta_0 + 2\sqrt{\theta_0(\theta_0 + u^2)}$ <sup>b</sup>	$3\theta_0 u$

<sup>a</sup> The temperature  $\theta$  is fixed to  $\theta_0$ .

<sup>b</sup> It could be expanded by the Taylor series expansion with respect to  $u = 0$  as  $\theta_0 + u^2 - u^4/(4\theta_0) + \dots$ .

The viscosity of the models is expressed by  $\nu = (1/\omega - 1/2)\sqrt{\theta_0}\Delta x/\sqrt{\zeta}$  [6] so that we use  $\omega = 1$  for the LBGK and the entropic models because they share their discrete velocities, and  $\omega = 4\sqrt{3} - 6$  for the parametric model with  $\zeta = 4$  to match viscosity. We use the results after 362 iterations for the LBGK and the entropic models, and 418 iterations [15] for the parametric model with  $\zeta = 4$ . The LBGK model gives the unstable oscillating result (gray solid line), while the parametric model with  $\zeta = 4$  (blue solid line) and the entropic model (red dashed line) provide the stable results. However, there is a disagreement on the velocity profile between the entropic model and the parametric model with  $\zeta = 4$ . The reason is that the entropic model does not satisfy  $\hat{\mu}_2 = \mu_2$  in contrast to the LBGK model and the parametric model with  $\zeta = 4$  as listed in Table I. Note that the moments  $\hat{\mu}_2$  and  $\hat{\mu}_3$  of the LBGK and the entropic models have the second-order accuracy in  $u$ , while the parametric model with  $\zeta = 4$  gives  $\hat{\mu}_3 = 4\theta_0 u$ . Therefore, we have performed two other simulations to investigate the effect of the moment errors of  $\hat{\mu}_2$  and  $\hat{\mu}_3$  of the models. The density, velocity, and temperature profiles of the LBGK model (white dashed), the parametric model with  $\zeta = 4$  (thick blue), and the entropic model (red dot-dashed) are shown in Fig. 3 for the initial density ratio  $\bar{\rho}_L/\bar{\rho}_R = 4$  and in Fig. 4 for  $\bar{\rho}_L/\bar{\rho}_R = 1.1$  in addition to the difference of density  $\Delta\bar{\rho}$  for the parametric model (thick blue) and for the entropic model (red dot-dashed) with respect to the LBGK model. We observe that the difference between the LBGK model and the parametric model with  $\zeta = 4$  is much less than the difference between the LBGK and the entropic models when  $\bar{\rho}_L/\bar{\rho}_R = 4$ . Instead of enhancing stability, the entropic model obtains serious damage in accuracy. The deviation of the entropic model is noticeable when

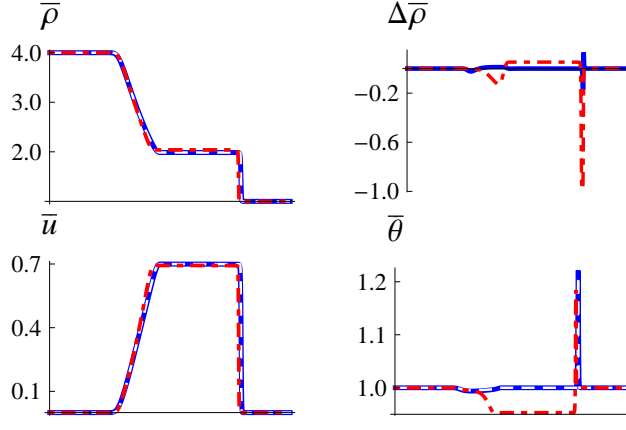


FIG. 3. (Color online) The density  $\bar{\rho}$ , velocity  $\bar{u}$ , and temperature  $\bar{\theta}$  profiles obtained by three discrete velocities with  $\bar{\rho}_L/\bar{\rho}_R = 4$  are drawn for the LBGK model (white dashed), the entropic model (red dot-dashed), and the parametric model with  $\zeta = 4$  (thick blue). The density difference  $\Delta\bar{\rho}$  for the parametric model (thick blue) and for the entropic model (red dot-dashed) with respect to the LBGK model is provided for clarity.

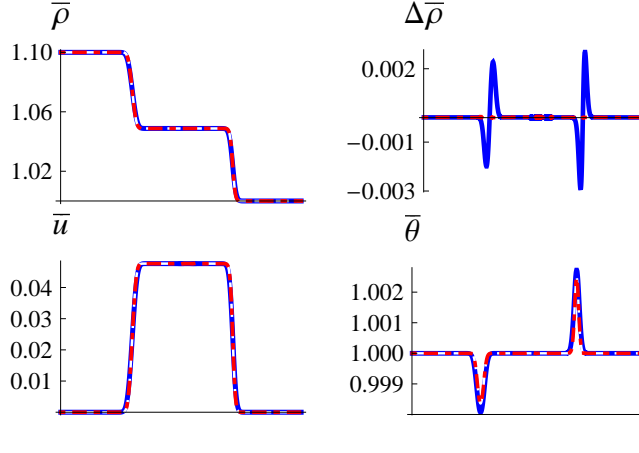


FIG. 4. (Color online) The simulation results with  $\bar{\rho}_L/\bar{\rho}_R = 1.1$  is drawn. The figure legends are the same to those of Fig. 3. The maximum  $\Delta\bar{\rho}$  of the parametric model with  $\zeta = 4$  with respect to the LBGK model is about 0.3%.

density ratio or flow velocity is relatively high. On the other hand, Fig. 4 shows that the differences are not easily observable when  $\bar{\rho}_L/\bar{\rho}_R = 1.1$  for all the models. The maximum differences of density and velocity between the parametric model with  $\zeta = 4$  and the LBGK model are about 0.3%.

The thermal flow simulation with the five velocities model derived in Eq. (4) shows that

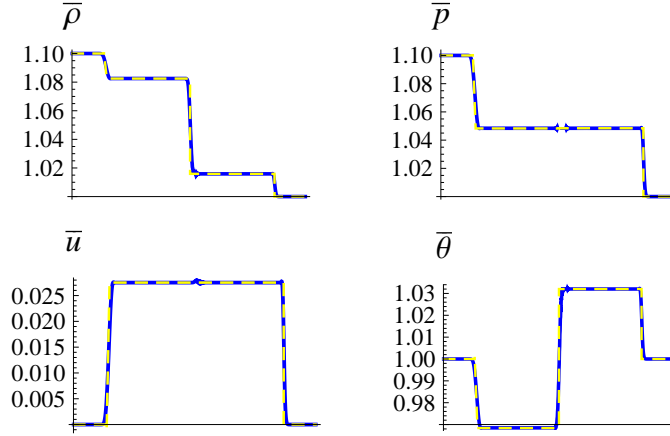


FIG. 5. (Color online) The simulation result obtained by the model of five discrete velocities (solid blue) and by the analytical solution of the Riemann problem for the Euler equations (yellow dashed) are drawn.

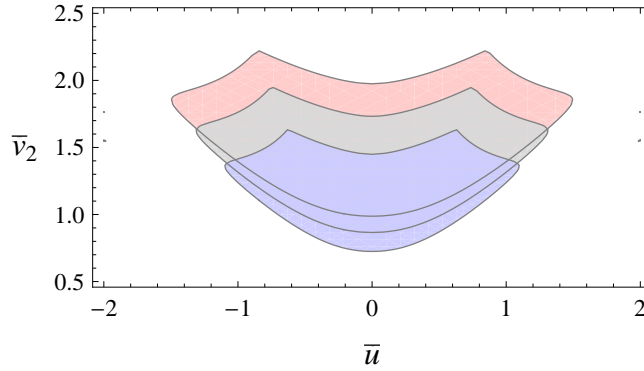


FIG. 6. (Color online) The contour plot of the redistribution rule  $r_i$  of the five discrete velocities is drawn when  $v_4 = 2v_2$ . The blue, gray, and red regions satisfy  $r_i \geq 0$  for  $\bar{\theta} = 0.7, 1$ , and  $1.3$ , respectively.

the use of isothermal approximation must be done carefully even for the case of  $\bar{u} \ll 1$ . Fig. 5 shows the result obtained by the parametric model (thick blue) of five discrete velocities with  $x = 1.4$  and  $y = 2x$ , which are selected by considering the ranges of  $\bar{u}$ ,  $\bar{\theta}$ , and  $\bar{v}_i$  that provide  $r_i \geq 0$  as in Fig. 6, and the analytical solution of the Riemann problem of the shock tube (yellow dashed) when  $\bar{\rho}_L/\bar{\rho}_R = 1.1$ . The significant difference is observed in comparison to the isothermal models of three discrete velocities. The flow velocity in the region of post-shock  $\bar{u}_{post}$  and the shock speed  $\bar{u}_{shock}$  obtained by the isothermal models are respectively over- and under-estimated by about 1.72 times than the one-dimensional thermal case and

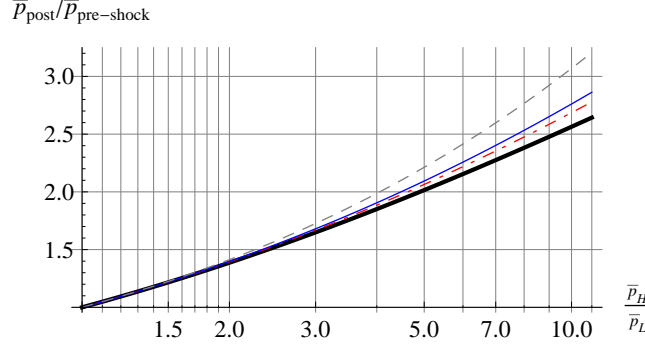


FIG. 7. (Color online) The ratio between the post- and pre-shock pressures with respect to the ratio between the high and the low pressures of an initial state is drawn by the solution of the Riemann problem of the shock tube for the Euler equations for the case isothermal (thick black), the cases of the one- (red dot-dashed), the two- (thin blue), and the three-dimensional spaces (gray dashed).

by about 1.28 times than the three-dimensional thermal case as well as the density profile having the well-known four steps instead of three steps, although the temperature fluctuation is about 3%. This is due to the heat capacity ratio  $\gamma$ ; the isothermal case  $\gamma = 1$  and the one-dimensional thermal case  $\gamma = 3$ . According to the Rankine-Hugoniot conditions, we obtain  $\bar{u}_{post}$  and  $\bar{u}_{shock}$  by  $\bar{u}_{post} = (\bar{p}_{post}/\bar{p}_{pre} - 1)/\bar{u}_{shock}$  and

$$\bar{u}_{shock} = \sqrt{\frac{(\gamma + 1)}{2}(\bar{p}_{post}/\bar{p}_{pre} - 1) + \gamma}$$

where  $\bar{p}_{post}$  and  $\bar{p}_{pre}$  are respectively pressures in post- and pre-shock regions. The ratio  $\bar{p}_{post}/\bar{p}_{pre}$  with respect to  $\bar{p}_H/\bar{p}_L$  is provided in Fig. 7 by the solution of the Riemann problem where  $\bar{p}_H$  and  $\bar{p}_L$  are respectively high and low pressures of initial states.

Lastly note that Eq. (2) also provides  $r_i$  upon an asymmetric set of discrete velocities. As an example, we have  $\{r_1, r_2, r_3\}$  as

$$\left\{1 - \frac{1 + \bar{u}^2 + \bar{v}\bar{u}}{2\bar{v}}, \frac{1 + \bar{u}^2 + 2\bar{u}\bar{v}}{3\bar{v}}, \frac{1 + \bar{u}^2 - \bar{u}\bar{v}}{6\bar{v}}\right\}$$

for corresponding discrete velocities  $\{0, \bar{v}, -2\bar{v}\}$ .

In conclusion, we have presented parametric discretized equilibrium distributions of the lattice Boltzmann method. The ranges of flow velocity and temperature providing  $r_i \geq 0$  vary with regulating discrete velocities as parameters. Thermal flows are simulated by only five on-lattice discrete velocities and 25 in one- and two-dimensional spaces, respectively.



The accuracy and the stability of the derived models have been tested and compared with existing models by the Riemann problem of the shock tube. The equilibrium distributions upon asymmetric sets of discrete velocities are also introduced.

## Appendix: Appendix

The redistribution rule  $r_i$  corresponding to a set of discrete velocities  $v_i$  for  $i = 1, 2, \dots, q$  is obtained by

$$\sum_{i=1}^q v_i^n r_i = \int_{-\infty}^{\infty} v^n F(v) dv \quad (\text{A.1})$$

for  $n = 0, 1, \dots, n^*$  where  $n^*$  is a desired order of accuracy,

$$F(v) = (2\pi\theta)^{(-d/2)} \exp[-\|v - u\|^2/(2\theta)],$$

$\theta = kT/m$ ,  $k$  the Boltzmann constant,  $T$  temperature,  $m$  mass of a particle,  $d$  dimension of space. In  $d$ -dimensional space with the Cartesian coordinate system,  $v^n$  is defined by  $\prod_{j=1}^d v_{x_j}^{n_j}$  for  $n = \sum_{j=1}^d n_j$  with non negative integers  $n_j$  where  $v_{x_j}$  is the  $j$ th coordinate component of  $v$  for  $j = 1, \dots, d$ . In one-dimensional space for  $n^* = q - 1$ , Eq. (A.1) can be expressed by  $R = V^{-1}M$  where

$$V = \begin{bmatrix} 1 & 1 & \dots & 1 \\ v_1 & v_2 & \dots & v_q \\ \vdots & \vdots & \ddots & \vdots \\ v_1^{q-1} & v_2^{q-1} & \dots & v_q^{q-1} \end{bmatrix}, R = \begin{bmatrix} r_1 \\ r_2 \\ \vdots \\ r_q \end{bmatrix}, M = \begin{bmatrix} \mu_0 \\ \mu_1 \\ \vdots \\ \mu_{q-1} \end{bmatrix}.$$

By using the explicit expression of  $V^{-1}$ , we can express  $r_i$  as

$$r_i = \frac{\sum_{n=0}^{q-1} \left( (-1)^n \mu_{q-1-n} \sum_{\substack{1 \leq j_1 < \dots < j_n \leq q-1 \\ j_1 \neq \dots \neq j_n \neq i}} v_{j_1} \dots v_{j_n} \right)}{\prod_{j \neq i} (v_i - v_j)}.$$

- 
- [1] U. Frisch, B. Hasslacher, and Y. Pomeau, Phys. Rev. Lett. **56**, 1505 (1986).
  - [2] G. R. McNamara and G. Zanetti, Phys. Rev. Lett. **61**, 2332 (1988).
  - [3] F. J. Higuera and J. Jimnez, EPL **9**, 663 (1989).
  - [4] S. Chen, H. Chen, D. Martnez, and W. Matthaeus, Phys. Rev. Lett. **67**, 3776 (1991).

- [5] H. Chen, S. Chen, and W. H. Matthaeus, Phys. Rev. A **45**, R5339 (1992).
- [6] Y. H. Qian, D. d’Humières, and P. Lallemand, EPL **17**, 479 (1992).
- [7] T. Abe, J. Comput. Phys. **131**, 241 (1997).
- [8] X. He and L.-S. Luo, Phys. Rev. E **55**, R6333 (1997).
- [9] X. Shan, X.-F. Yuan, and H. Chen, J. Fluid Mech. **550**, 413 (2006).
- [10] J. W. Shim, Phys. Rev. E **87**, 013312 (2013).
- [11] P. C. Philippi, L. A. Hegele, L. O. E. dos Santos, and R. Surmas, Phys. Rev. E **73**, 056702 (2006).
- [12] J. W. Shim, Phys. Rev. E **88**, 053310 (2013).
- [13] J. W. Shim and R. Gatignol, Z. Angew. Math. Phys. **64**, 473 (2013).
- [14] S. Ansumali, I. V. Karlin, and H. C. Öttinger, EPL **63**, 798 (2003).
- [15] The time mismatch is only about  $0.0016(\approx 362 \times 2/\sqrt{3} - 418)$  iteration.